Supplementary Information

Chiroptical detection and mutation analysis of cancer-associated extracellular vesicles in microfluidic devices

Yoon-Tae Kang[1,‡], Ji-Young Kim[1,‡], Hee-Jeong Jang[1], Chung-Man Lim[1], Colin Palacios-Rolston[1], Emma Purcell[1], Sarah Owen[1], Chitra Subramanian[1], Rishindra Reddy[3], Shruthi Jolly[4], Nithya Ramnath[5], Sunitha Nagrath[1,2,], Nicholas A. Kotov[1,*]*

[1]Department of Chemical Engineering and Biointerfaces Institute, University of Michigan, 2800 Plymouth Road, NCRC B10-A184, Ann Arbor, MI 48109, USA

[2]Roger Cancer Center, University of Michigan, 1500 E Medical Center Dr. Ann Arbor, 48109

[3]Michigan Medicine Thoracic Surgery Clinic, Taubman Center, 1500E Medical Center Dr. SPC 5344, Ann Arbor, MI, 48109 USA

[4]Radiation of Oncology, University of Hospital, University of Michigan, 1500 E Medical Center Dr. Ann Arbor, MI, 48109, USA

[5]Department of Internal Medicine, University of Michigan, Ann Arbor, MI, 48109 USA

*Correspondence: Dr. Nicholas A. Kotov (kotov@umich.edu) and Dr. Sunitha Nagrath (snagrath@umich.edu)

[*] Co-corresponding authors

[‡] Two authors contributed equally to this work

Contents

Figures & Table

S1. The size distribution and ζ-potential of the chiral AuNP probe

The average diameter and ζ-potential determined by dynamic light scattering is 113.7 nm and 11.4 mV, respectively.

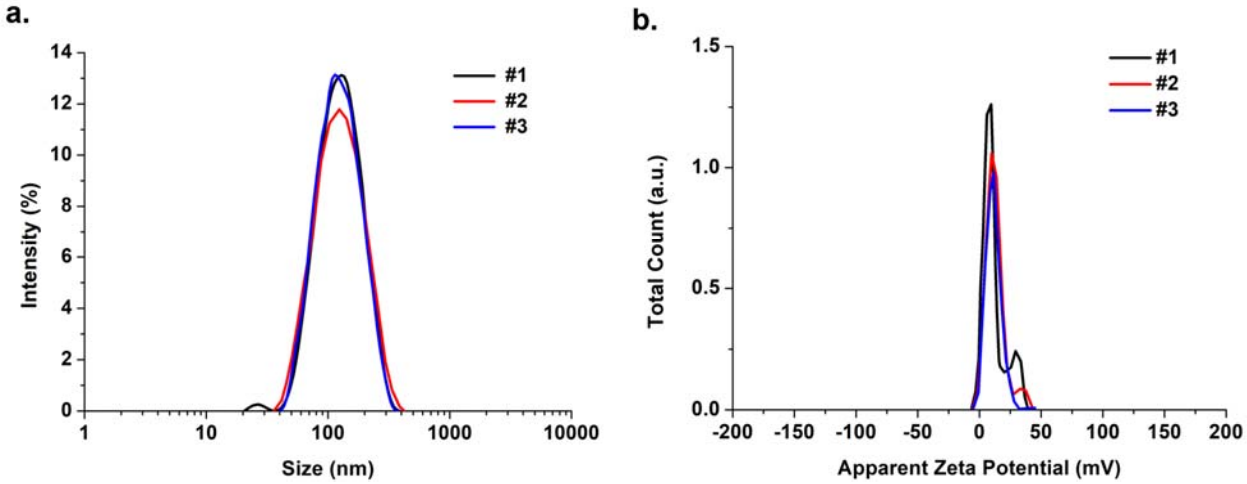

Figure S1. Size distribution and ζ-potential of the chiral AuNPs: (a) Size distribution by dynamic light scattering (DLS) and **(b)** ζ-potential of the chiral AuNP probe.

S2. Electron Tomography of L-AuNP

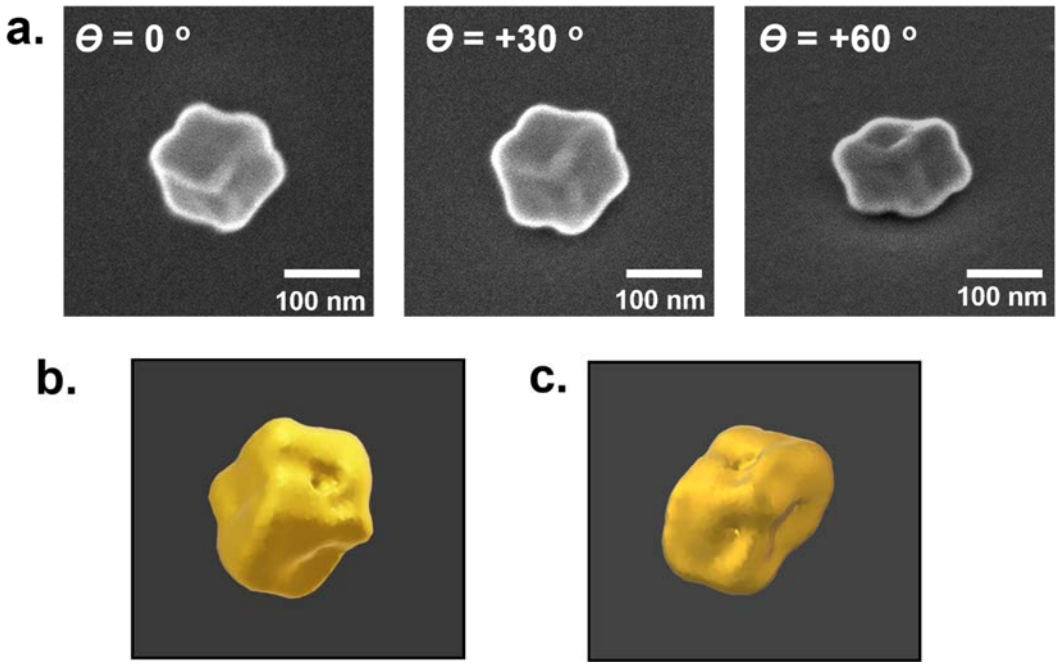

Figure S2. Three-dimensional morphology of Chiral AuNPs: (a) Tilted series of SEM images for *L*-Cys AuNPs. (b,c,) Top (b) and side (c) view of reconstructed 3D electron tomography of the *L*-Cys AuNPs.

S3. Three-dimensional model structures of AuNP enantiomer

The three-dimensional structure of AuNP enantiomers were constructed based on the morphology of the AuNPs observed by electron microscopies. The tilted SEM image series (Fig. S2a) showed that the AuNPs are the plate-like AuNPs with roughly estimated thickness of 100 nm. The two enantiomer model structures were constructed by importing distorted cuboid structures with propeller-like edges (edge length =150 nm). The structures are mirrored to each other on yz plane as shown in Fig. S2b and c. The 3D developed models have been imported into the electromagnetic simulation. (Fig. 1f-h) As expected, AuNPs fixed on the substrate showed considerable red shift and broadening in spectral range of the chiroptical bands compared to the chiral Au NPs colloid sample. Such change in chiroptical activities is often observed in deposition of anisotropic NPs due to its limited angle to the incidence as well as environmental dielectric change in solid states.

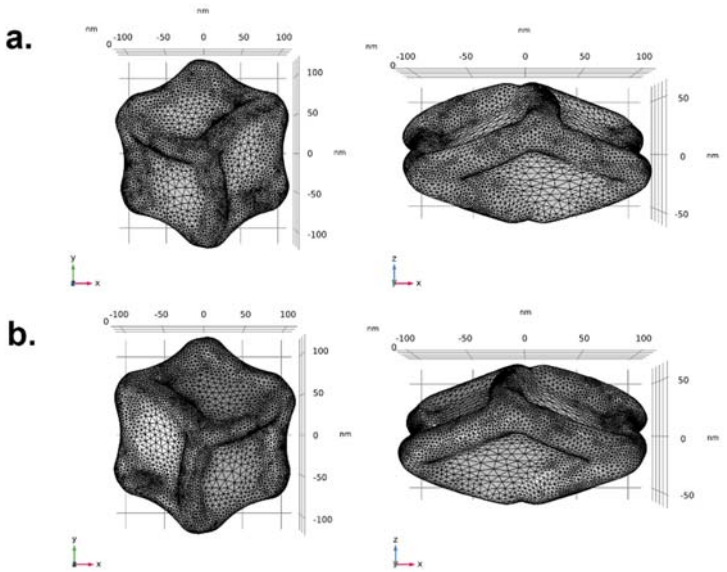

Figure S3. Three-dimensional enantiomer structure models of AuNPs: Top (left) and side (right) view of the enantiomer AuNP models which represents *L*-Cys (a) and *D*-Cys (b) AuNPs, respectively.

S4. Evaluation Criteria for the Present Devices and Definitions

The recovery rate is the fraction of release resultant to the sum of the capture effluent and release resultant. If we do not know the initial concentration of sample but want to know the isolation tendency of the present device, a simpler version of capture/release efficiency is 'recovery rate' derived only from capture effluent and release resultant concentrations. It is calculated as follow.

$$\boldsymbol{Recovery\ Rate}\ (\%) = \left[\frac{(concentration\ of\ exosome-sized\ vesicles\ in\ release\ resultant)}{(concentration\ of\ exosome-sized\ vesicles\ in\ capture\ effluent + release\ resultant)}\right] * 100\%$$

In order to evaluate whether the present device captures purified exosomes from the heterogeneous samples, we calculated the purity of the sample, the fraction of the concentration in exosome sized vesicles compared to whole concentration. Whole concentration values came directly from NTA result, and the concentrations of exosome sized vesicles were re-calculated from the NTA raw data.

$$\boldsymbol{Purity}\ (\%) = \left[\frac{(concentration\ of\ exosome-sized\ vesicles\ in\ sample)}{(concentration\ of\ whole\ vesicles\ in\ sample)}\right] * 100\%$$

Particle-size distribution (PSD) analysis was used to profile our NK-Exo from clinical samples. The PSD is a list of values of a mathematical function that defines the relative number of particles present according to size. This includes the particle size span width, *D10*, *D50* and *D90*, as known as three point specification or *D-value*. More specifically, those three *D-values* indicate the diameter of the particle at 10%, 50% and 90% of the cumulative distribution. For example, if *D50* is 150nm, it means that 50% of the particles in the sample from NTA are bigger than 150 nm and another 50% are smaller than 150nm.

S5. Fabrication and surface modification of CDEXO chip

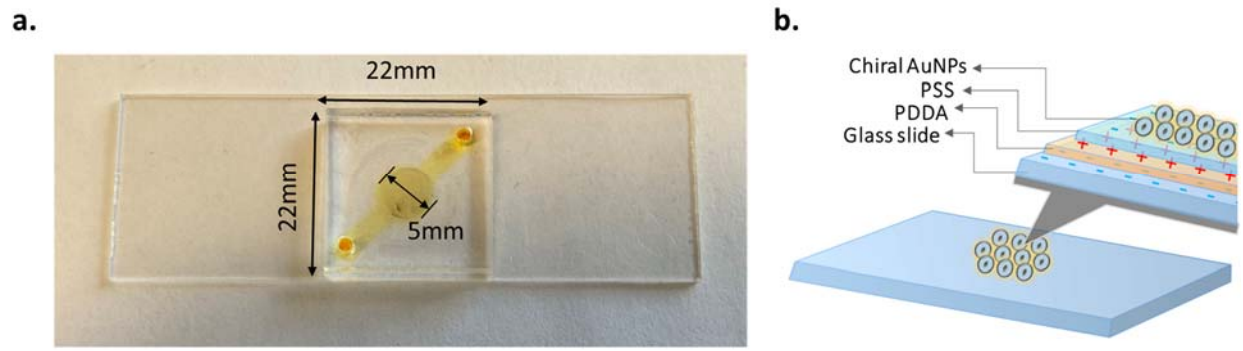

Figure S4. CDEXO microfluidic device: (a) the fabricated CDEXO device with dimensions; **(b)** information of each layer on CDEXO device.

S6. The computational model for chiral Au NP – exosome complex

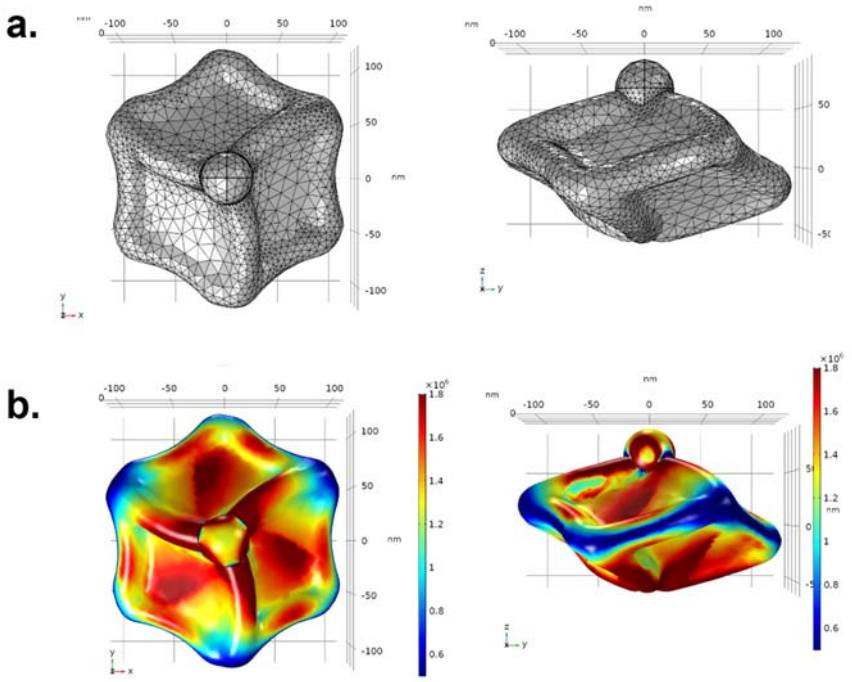

Figure S5. Three-dimensional L-Cys AuNP model with exosome-mimic dielectric particle: Top (left) and side (right) view of (a) 3D model structure of AuNP-exosome complex and (b) averaged extinction surface map under CPL at wavelength of 550 nm.

S7. CD profile of two different lung cancer exosomes using CDEXO

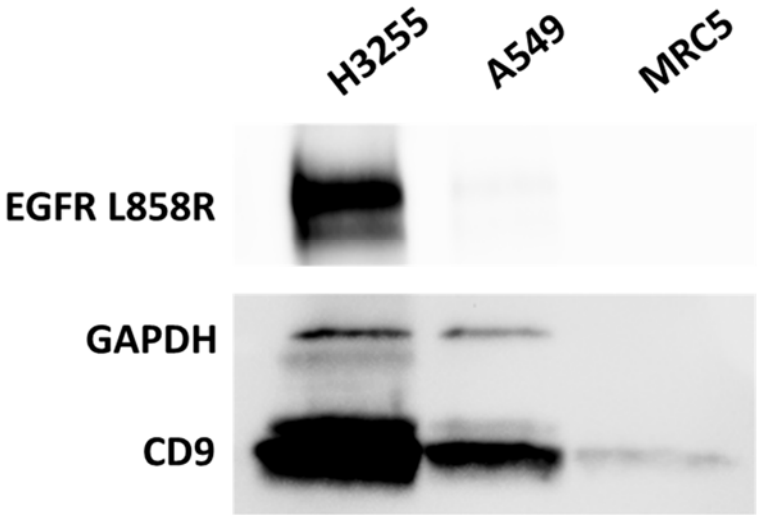

Figure S6. Western blot analysis of exosome from three different cancer/normal lung cells carrying different EGFR mutations

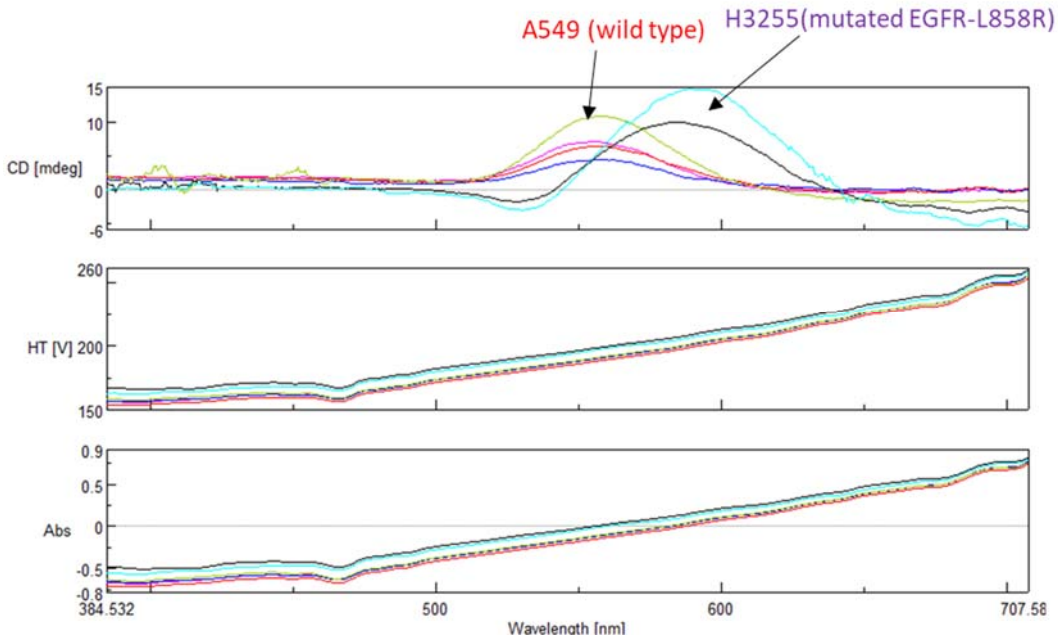

Figure S7. CD signals of two different lung cancer cell line derived exosomes on CDEXO device

S8. CD profile of lung cancer patients

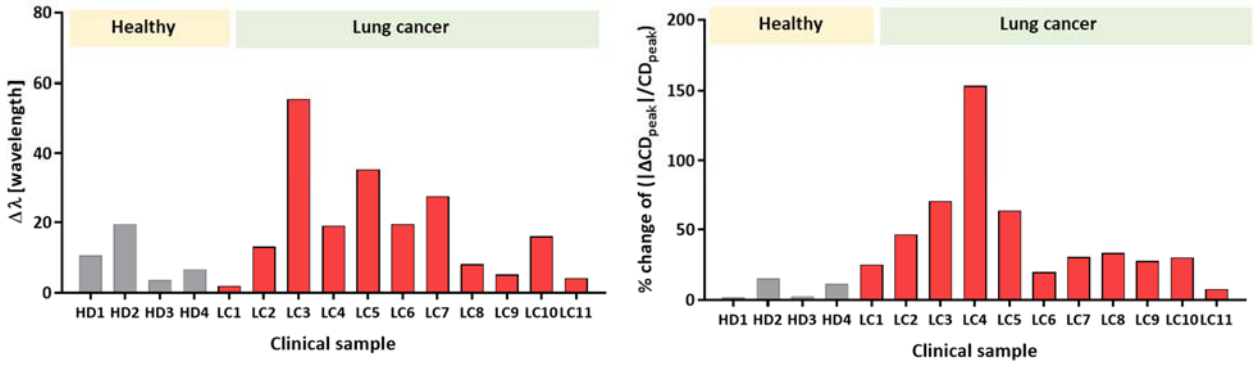

Figure S8. Comparison of CD signal between healthy and lung cancer patients: (a) amount of CD-peak shift for each sample; (b) percentage of change in CD peak magnitude after exosome isolation comparing to baseline CD-peak for each sample

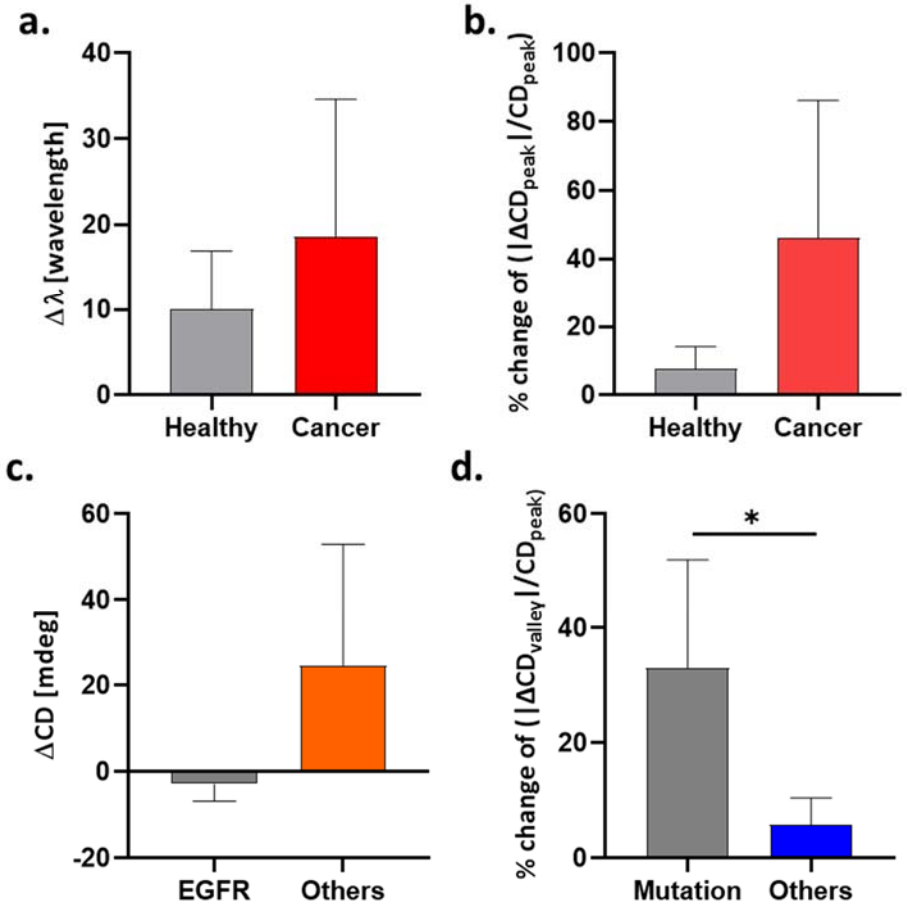

Figure S9. Average circular dichroism spectra change between clinical groups

S9. Patients information

Table S1. Clinical information of the patient samples

Cancer Type	Sample ID	Sample description						
		Sex	Age	Stage	Adenocarcinoma subtype	Mutation	Treatment	Tumor origin
Lung cancer patient	***LP1***	Male	83	III	Squamous cell	EGFR Exon 19 deletion	Carboplatin, Paclitaxel, radiation	Right lower lobe
	LP2	Female	65	III	Squamous cell	None	Carboplatin, Paclitaxel, radiation	Left lower lobe
	LP3	Female	81	III	Squamous cell	None	Carboplatin, Paclitaxel, radiation	Right upper lobe
	LP4	Male	74	III	Squamous cell	None	Carboplatin, Paclitaxel, radiation	Left lower lobe
	LP5	Female	58	IV	EGFR	EGFR mutation	Carboplatin/ pemetrexed	Left upper lobe
	LP6	Female	61	IV	EGFR	EGFR Exon 19 deletion	Tarceva	Left upper lobe
	LP7	Female	78	IV	EGFR	EGFR mutant AC with T790M mutation	Osimertinib	Right lower lobe
	LP8	Female	55	IV	ROS1	ROS1 Mutation	Crizotinib	Neck
	LP9	Male	58	IV	ALK	None	Alectinib	Right lower lobe
	LP10	Female	61	IV	EGFR	EGFR mutant AC with T790M mutation	Osimertinib	Left upper lobe
	LP11	Male	62	IV	EGFR	EGFR Exon 19 deletion	Afatinib	Right upper love